Groundwater

Pressure Buildup and Brine Migration During CO_2 Storage in Multilayered Aquifers

by Abdullah Cihan[1], Jens T. Birkholzer[2], and Quanlin Zhou[2]

Abstract

Carbon dioxide injection into deep saline formations may induce large-scale pressure increases and migration of native fluid. Local high-conductivity features, such as improperly abandoned wells or conductive faults, could act as conduits for focused leakage of brine into shallow groundwater resources. Pressurized brine can also be pushed into overlying/underlying formations because of diffuse leakage through low-permeability aquitards, which occur over large areas and may allow for effective pressure bleed-off in the storage reservoirs. This study presents the application of a recently developed analytical solution for pressure buildup and leakage rates in a multilayered aquifer-aquitard system with focused and diffuse brine leakage. The accuracy of this single-phase analytical solution for estimating far-field flow processes is verified by comparison with a numerical simulation study that considers the details of two-phase flow. We then present several example applications for a hypothetical CO_2 injection scenario (without consideration of two-phase flow) to demonstrate that the new solution is an efficient tool for analyzing regional pressure buildup in a multilayered system, as well as for gaining insights into the leakage processes of flow through aquitards, leaky wells, and/or leaky faults. This solution may be particularly useful when a large number of calculations needs to be performed, that is, for uncertainty quantification, for parameter estimation, or for the optimization of pressure-management schemes.

Introduction

Carbon dioxide capture combined with geologic storage (CCS) in suitable subsurface formations has been suggested as one of several important strategies for solving the world's carbon-emission problem (Pacala and Socolow 2004; IPCC 2005). However, the volumes of compressed supercritical CO_2 to be sequestered in industrial-scale sequestration projects are very large, potentially creating far-ranging pressure buildup and brine displacement in deep CO_2 storage formations (Van der Meer 1992; Nicot 2008; Birkholzer and Zhou 2009; Birkholzer et al. 2009; Zhou and Birkholzer 2011). Injection-induced pressure changes can cause migration of brine from the storage formation into other parts of the subsurface where permeable pathways exist, such as old wells (Gasda et al. 2004; Celia et al. 2011) or permeable faults (Rutqvist et al. 2007, 2008). Such migration of brine (or CO_2) out of the storage region is defined as leakage in the geologic CO_2 storage context (Oldenburg et al. 2004), although in this paper we also use the term "leaky" in the classic hydrology context in which it suggests one or more permeable pathways, for example, through an aquitard (Freeze and Cherry 1979).

Understanding and predicting the environmental impacts of leakage and other large-scale displacements of resident brine caused by CCS operations require modeling/analysis tools of considerable complexity (Celia et al. 2011). First, the spatial domains affected by pressure

[1]Corresponding author: Earth Sciences Division, Lawrence Berkeley National Laboratory, University of California, Berkeley, CA 94720; acihan@lbl.gov

[2]Earth Sciences Division, Lawrence Berkeley National Laboratory, University of California, Berkeley, CA 94720.

Received November 2011, accepted June 2012.

doi: 10.1111/j.1745-6584.2012.00972.x

changes can extend over thousands of square kilometers in the horizontal direction (Birkholzer and Zhou 2009; Zhou et al. 2010), while often comprising multiple layers of high-permeability (aquifer) and low-permeability (aquitard) formations in the vertical direction. While the aquitards generally considered as caprock for CO_2 sequestration are often nearly impenetrable (due to very small permeability and high capillary entry pressure), the pressurized brine in the storage formation can migrate into aquitards in a slow process referred to as "diffuse" leakage (as opposed to "focused" leakage along leaky wells or faults). The diffuse leakage rate is usually very small; however, over long times and large areas, diffuse leakage can account for significant volumes of water transferred from the storage formation into over- or underlying formations. Birkholzer et al. (2009) demonstrated the importance of this transfer in mitigating pressure effects ("pressure bleed-off") in the storage formation and concluded that aquitards should be accounted for in large-scale pressure evaluations.

Second, the necessity of evaluating large spatial domains is often accompanied by the need for considering hundreds or even thousands of local features, such as injection or extraction wells as well as potentially leaky wells and faults. Regional saline aquifers, such as the Mount Simon Sandstone in the Illinois Basin, may someday host numerous individual CO_2 storage projects (Birkholzer and Zhou 2009; Person et al. 2010; Zhou et al. 2010), and each of these projects could require more than one injection well. Recent studies have discussed the possibility of brine extraction from CO_2 storage formations to better control subsurface pressure increases and thereby achieve higher dynamic storage capacity (Bergmo et al. 2011; Court et al. 2011). Depending on the design and purpose of such brine extraction, several pumping or pressure-relief wells may be needed in addition to injection wells (Buscheck et al. 2011). In areas with a long history of oil and gas production, enormous numbers of wells have been drilled into the deep subsurface for exploration and production. North America alone has been perforated by millions of oil and gas wells since the late 1800s (IPCC 2005). For example, according to a spatial analysis conducted in the Alberta Basin (Gasda et al. 2004), well densities may range from 0.15 to 17 wells per square kilometer for oil and gas-pool areas with low to very high well population. The main concern for CCS in such areas is the presence of abandoned legacy wells that could potentially act as pathways for focused leakage. Many of these wells may be decades old, with uncertain properties and undocumented depth (Gasda et al. 2004).

The numerical simulation of regional-scale flow processes in large multilayered model domains combined with local flow phenomena in/near multiple wells and/or faults can easily generate very challenging and sometimes impractical computational requirements, particularly if research goals of uncertainty estimation and model calibration call for numerous, repeated simulation runs. While researchers have used high-performance computing techniques for basin-scale evaluations of CO_2 sequestration (Yamamoto et al. 2009; Zhou et al. 2010), inclusion of hundreds or even thousands of leaky wells has so far proven prohibitive because of computational requirements. As an alternative to numerical simulation models, analytical or semi-analytical solutions can be particularly useful when dealing with a large number of injection and leaky wells because they are very efficient with regard to calculation time and memory requirements and do not require spatial (or temporal) discretization.

A set of analytical and semi-analytical solutions for CO_2 storage applications with leaky wells has been developed over the past several years by researchers at Princeton University and the University of Bergen. Their vertically integrated sharp-interface solution for CO_2 plume behavior without phase transitions (Nordbotten and Celia 2006), and with an effective-permeability and Darcy flow treatment for fluid flow along leaky wells (Nordbotten et al. 2009), allows efficient representation of an arbitrary number of aquifers and leaky wells (Celia and Nordbotten 2009; Celia et al. 2011). However, in this solution set, aquitards are assumed to be impermeable except for possible flows along existing wells; thus, it is not possible to consider diffuse leakage processes.

In the present work, we complement the above-mentioned suite of computational models for CO_2 sequestration applications by applying a recently developed analytical solution for single-phase flow in multilayered systems with diffuse and focused brine leakage (Cihan et al. 2011). The basic consideration is that the brine pressurization and migration processes outside of the CO_2 plume region can be reasonably well described by single-phase flow models—without accounting for local two-phase and variable density effects—simply by representing the injection of CO_2 as an equivalent volume of saline water (Nicot 2008). The solution described by Cihan et al. (2011) solves for pressure change and fluid flow in a multilayered system of any number of aquifers, leaky aquitards, injection/pumping wells, and leaky wells. Because we focus on brine leakage, we avoid the concerns about two-phase flow and strongly varying property change limitations of the analytical solutions associated with CO_2 leakage.

To demonstrate application of the analytical solution by Cihan et al. (2011), we consider a hypothetical scenario of CO_2 sequestration in a multilayered sequence of aquifers and aquitards with multiple injection wells, multiple leaky wells, and a leaky fault. The injection rate corresponds to the amount of CO_2 captured from a large coal-fired power plant operating over a 50-year period. Pathways for focused leakage are located about 20 km from the five CO_2 injection wells, and are far away from the maximum CO_2 plume but close enough to experience considerable pressure buildup in the injection formation and thus to create brine leakage risk to shallow groundwater sources. We use the application example to elucidate the (1) pressure response in the several aquifers of the multilayered system, (2) the interplay between diffuse and focused leakage, and (3) the sensitivity of

these results to aquitard and well permeabilities. While this scenario does not correspond to any particular site, it is broadly representative of sedimentary basin sequences under investigation for large-scale geologic CO_2 sequestration.

The paper is organized as follows. First, we briefly review the analytical solution developed by Cihan et al. (2011), and explain a few modifications made to allow for different types of well and fault leakage. To demonstrate that a single-phase flow model can sufficiently represent far-field flow processes, we compare the analytical solution to the results obtained by Birkholzer et al. (2009) using multiphase flow modeling of CO_2 injection into a multilayered sequence. Next, we introduce the hypothetical CO_2 sequestration scenario and focus our discussion on the pressure response and diffuse-vs.-focused leakage rates. We consider different leakage cases and related sensitivities, with different aquitard permeabilities, different well leakage types and well properties, and the absence/presence of a leaky fault.

Overview of the Analytical Solution Method

Cihan et al. (2011) presented a generalized framework for analytically solving the coupled focused and diffuse flow of a single-phase fluid, in a multilayered system comprising an arbitrary number of aquifers and alternating aquitards. While all aquifers and aquitards are assumed homogeneous, with uniform thickness and infinite extent, each aquifer and aquitard may have different thicknesses and hydraulic properties. Fluid flow is horizontal in the aquifers and vertical in the aquitards, which is considered a valid assumption as long as the ratio of hydraulic conductivity between the aquifers and the aquitards is larger than 100 (Neumann and Witherspoon 1969). Leaky wells are represented as Darcy-type flow pathways with segment-wise property (well radii, permeability, screened/cased in well-aquifer segments, plugged/unplugged in well-aquitard segments) variation, where segments correspond to intersections of each well with layers of the multilayered system.

The equations of horizontal groundwater flow in the aquifers are coupled by the vertical-flow equations in the aquitards and the flow-continuity equations in the leaky wells. The governing partial differential equations for single-phase flow in aquifers and aquitards (see Eqs. 1a and 2a in Cihan et al. 2011) are transformed into the Laplace domain, and the resulting coupled system of ordinary differential equations are solved using the eigenvalue analysis method. The generalized solution for hydraulic head buildup or drawdown in the Laplace domain for a system of N aquifers, N_I injection wells, and N_L leaky wells is developed using the superposition principle. (Note that the entire system is initially assumed to be at hydrostatic equilibrium.) The Stehfest numerical Laplace inversion method (Stehfest 1970a, 1970b) is applied to convert the solutions obtained in the Laplace domain into the real-time domain. Readers are referred to Cihan et al. (2011) for further details of the solution method and description of a FORTRAN program developed for computing the general solution. Starting from the solution described in Cihan et al. (2011), we have since made modifications to the general solution to allow for (1) impermeable aquitards (focused leakage only problem), (2) screened well-aquifer segments (fully interacting with intervening aquifers), (3) cased well-aquifer segments (no flow in lateral direction), (4) plugged well-aquitard segments (no flow in vertical direction), (5) plugged with no flow or flowing/artesian wells with zero head change at the top.

In one of the following simulations, we use the leaky-well feature to approximate hydraulic-head changes and leakage in a vertically conductive fault zone. Shan et al. (1995) presented explicit analytical solutions in Cartesian coordinates for leakage through a fault intersecting a system of two aquifers separated by an aquitard. In Shan et al. (1995), the leaky fault is represented as a line source with a finite vertical transmissivity, while aquifers and aquitards are homogeneous and isotropic with infinite horizontal extent. In this study, to represent the fault zone, an array of several leaky wells is geometrically arranged in a line pattern, with their number and radii selected in such a way that the total cross-sectional area of the wells and the distance covered by the wells match the fault geometry. (For instance, assuming a fault with L_f length and W width, the required number and radii of the leaky wells are $L_f\,\pi/(4W)$ and $2W/\pi$, respectively.) This approximate fault representation involves several simplifying assumptions, including the assumption that heterogeneity and anisotropy inside the fault zone can be neglected, and we are only interested in vertical flow along the fault zone, and that the presence of the fault zone does not change the horizontal conductivity within the aquifers intersected by the fault as assumed by Shan et al. (1995).

Accuracy of the Single-Phase Assumption

This section assesses the suitability, for large-scale CO_2 injection, of using a single-phase solution to represent far-field pressure changes and brine leakage. It is assumed that the buoyancy, capillary effects, and changes in hydraulic properties within the two-phase zone have a small impact on pressure buildup and fluid flow outside of this zone (Nicot 2008). When applying the analytical model by Cihan et al. (2011) to a CO_2 injection problem, additional assumptions are required, for example, that CO_2 is injected over the entire aquifer thickness in a multilayered system, and that dissolution and other mass-transfer processes among the phases can be neglected. In addition to these assumptions, the volume of the injected fluid in the single-phase flow model needs to be equivalent to the volume of CO_2 to be sequestered. For CO_2 injection with a constant mass flow rate, the equivalent volumetric rate needs to be recalculated as a function of time, as fluid properties change with injection-induced pressure increases.

We apply the analytical solution of Cihan et al. (2011) to a multiphase simulation study conducted by Birkholzer et al. (2009) using the multiphase simulator TOUGH2/ECO2N (Pruess 2005). Birkholzer et al. (2009) investigated the pressure buildup and diffuse leakage over 30 years from industrial-scale injection of CO_2 at a rate of 1.52 million tons per year. A radially symmetric multilayered system with eight aquifers and seven alternating aquitards is considered, bounded at the top and bottom by impermeable formations (Figure 1). (Radius of the numerical model domain, R, is 200 km.) Aquifers and aquitards are numbered 1 through 8 and 1 through 7, respectively, from bottom to top; injection is into the bottom of Aquifer 1. The four bottom aquifers have high salinity, while the top four aquifers are considered groundwater resources. All layers are horizontal, homogeneous, and isotropic. Each aquifer has 60 m thickness, 10^{-13} m^2 permeability, 20% porosity, and 4.5×10^{-10} Pa^{-1} pore compressibility. Each aquitard has 100 m thickness, 10^{-18} m^2 permeability (base case), 15% porosity, and 9×10^{-10} Pa^{-1} pore compressibility. (Note that a typographical error exists in Table 1 of Birkholzer et al. [2009] which reported 5% porosity for aquitards instead of the correct 15%.) The total thickness of the multilayered model system is 1180 m.

In Birkholzer et al. (2009), density and viscosity of the fluids were varied with pressure, temperature, and salinity, although transient changes in temperature were not simulated. Molecular diffusion and mechanical dispersion of dissolved CO_2 in brine were also neglected. Our analytical-solution calculations consider the same initial variability of the fluid properties as a function of depth, averaged over the thicknesses of aquifers and aquitards, so that layer-wise hydraulic properties (hydraulic conductivity, L/T, and storativity, $1/L$) could be calculated. Table 1 lists the fluid properties from the bottom layer (Aquifer 1) to the top layer (Aquifer 8) used for calculating storativity and hydraulic conductivity values for the analytical model.

Note that CO_2 injection in the Birkholzer et al. (2009) model occurs only over the 30 m bottom length of the storage aquifer (half of aquifer thickness) and was approximated by a cylindrical injection zone of 50 m radius. In our analytical solution study, the injection source is also represented by a cylindrical zone with a 50-m radius, but injection occurs over the entire aquifer thickness. The volumetric injection rate corresponding to the constant mass injection rate changes slightly during injection, owing to changes in fluid properties as the pressure increased. This time-dependent, volumetric injection rate is represented using 17 time periods. Because of the relatively modest pressure changes, and the correspondingly rather minor changes in CO_2 density, we find that even a constant injection rate (5078 m^3/d as an average, corresponding to a CO_2 density of approximately 820 kg/m^3) provides sufficiently accurate results for both the pressure increases and diffuse leakage rates.

Figure 2a presents temporal changes in head buildup within the storage aquifer at 10.5 km distance from the center of the injection zone for different aquitard permeability values ($k' = 10^{-17}$, 10^{-18}, 10^{-19} m^2). Head buildup decreases with decreases in the aquitard permeability. Dashed lines show the multiphase TOUGH2/ECO2N model results, and solid lines represent the analytical model results. The pressure-buildup values produced

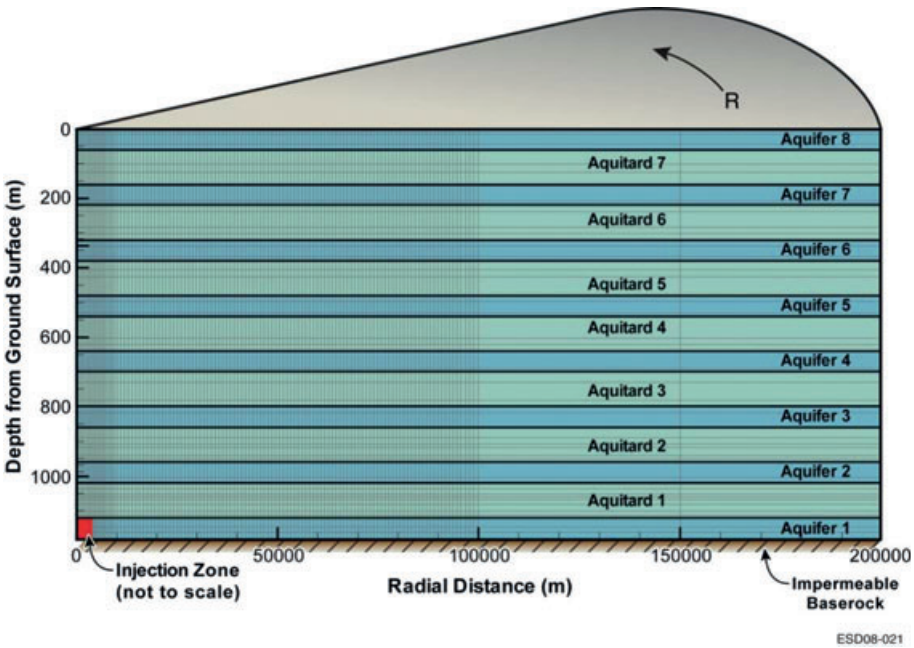

Figure 1. Schematic showing the radially symmetric model domain in Birkholzer et al. (2009), with Aquifer 1 for CO_2 storage and overlying aquifer/aquitard sequence. Aquifers 1 through 4 are saline aquifers, while Aquifers 5 through 8 are freshwater aquifers.

Table 1
Fluid Properties in Aquifers and Aquitards

Layer	Density(kg/m ^{3})		Viscosity (Pa s)		Brine Compressibility (Pa^{-1})	
	Aquifer	Aquitard	Aquifer	Aquitard	Aquifer	Aquitard
1 (bottom)	1095.63	1078.41	9.16×10^{-4}	8.90×10^{-4}	3.37×10^{-10}	3.52×10^{-10}
2	1062.46	1046.52	8.69×10^{-4}	8.54×10^{-4}	3.67×10^{-10}	3.83×10^{-10}
3	1030.41	1021.50	8.42×10^{-4}	8.49×10^{-4}	4.01×10^{-10}	4.13×10^{-10}
4	1013.32	1004.78	8.59×10^{-4}	8.70×10^{-4}	4.25×10^{-10}	4.38×10^{-10}
5	999.26	999.31	8.89×10^{-4}	9.22×10^{-4}	4.49×10^{-10}	4.52×10^{-10}
6	999.36	999.37	9.58×10^{-4}	9.99×10^{-4}	4.55×10^{-10}	4.58×10^{-10}
7	999.37	999.34	1.04×10^{-3}	1.08×10^{-3}	4.62×10^{-10}	4.65×10^{-10}
8 (top)	999.28		1.12×10^{-3}		4.69×10^{-10}	

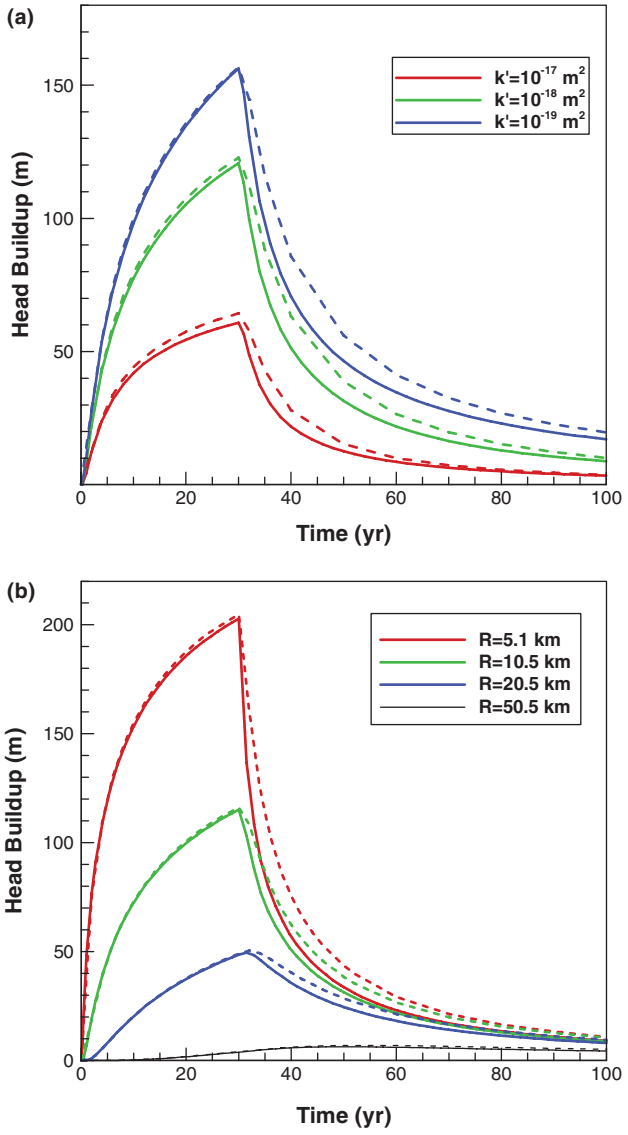

Figure 2. Head buildup in the storage aquifer (aquifer 5) as a function of time and (a) permeability at 10 km distance, and (b) radial distance. Dashed lines represent the numerical simulation results; solid lines represent the analytical solution results.

by the TOUGH2/ECO2N simulation (Birkholzer et al. 2009) were converted into head-buildup values, in order to compare with the analytical solution. Figure 2b presents head buildup changes within the storage aquifer for $k' = 10^{-18}$ m^2 at selected locations outside of the two-phase CO_2-brine zone. The analytical solution with single-phase flow matches the TOUGH2/ECO2N results reasonably well, particularly during the injection period. After injection stops, the analytical solution predicts a slightly faster pressure decrease than the TOUGH2/ECO2N simulation. The delayed response in the two-phase model occurs primarily as a result of the larger fluid compressibility of CO_2 in the two-phase zone, which is not taken into account in the single-phase analytical model. Note that the analytical solution significantly overpredicted the head buildup inside the CO_2 plume zone. Results from the two-phase model suggest that for $k' = 10^{-18}$ m^2, the CO_2 plume reached about 2 km distance at 30 years and extended to 2.8 km at 100 years. At 100 years, about 92% of CO_2 injected stayed in the supercritical phase, and the rest was

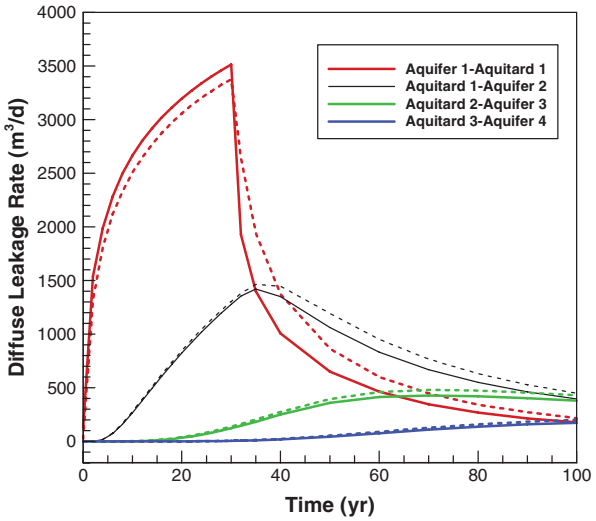

Figure 3. Diffuse leakage rate as a function of time at selected aquifer-aquitard interfaces. Dashed lines represent the numerical simulation results; solid lines represent the analytical solution results.

dissolved in the aqueous phase. Figure 3 shows the total rate of vertical fluid flow (diffuse leakage) at the interfaces between selected aquifers and aquitards (i.e., Aquifer 1 to Aquitard 1, Aquitard 1 to Aquifer 2, Aquitard 2 to Aquifer 3, and Aquitard 3 to Aquifer 4), integrated over the entire interface area. Aquitard permeability in this case is equal to 10^{-18} m^2. Again, we see reasonable agreement between single-phase and two-phase results. The analytical solution slightly overestimates diffuse brine leakage out of the storage formation during injection, in part because it does not account for the reduced effective permeability of brine within the two-phase zone. Consistent with the head results in Figure 2b, the single-phase solution shows a faster reduction in leakage rates after injection ceases, because the effective compressibility of the fluids in the two-phase zone is underestimated.

Figure 4 shows vertical profiles of pressure buildup for selected locations at 30 and at 100 years. Pressure perturbations occur not only in the storage formation, but also in the overlying formations, a result of slow diffuse leakage through the low-permeability aquitards. At the end of injection (30 years), the single-phase analytical model accurately represents the vertical distribution of pressure changes, while at 100 years, the pressure buildup is slightly lower than in the two-phase model. As mentioned before, this latter discrepancy is caused by the inaccurate fluid compressibility assumed by the analytical solution within the two-phase zone. Overall, pressure buildup (outside of the CO_2 plume) and diffuse leakage results for the two solution methods compare favorably. On the average over 100 years, the head buildup predicted by the analytical solution and numerical solution differs by less than 10%, while the diffuse leakage rate predictions differ by less than 15%. We conclude that far-field pressure-buildup behavior and brine-leakage processes associated with a large-scale CO_2 injection project can be approximated by single-phase flow calculations with reasonable accuracy.

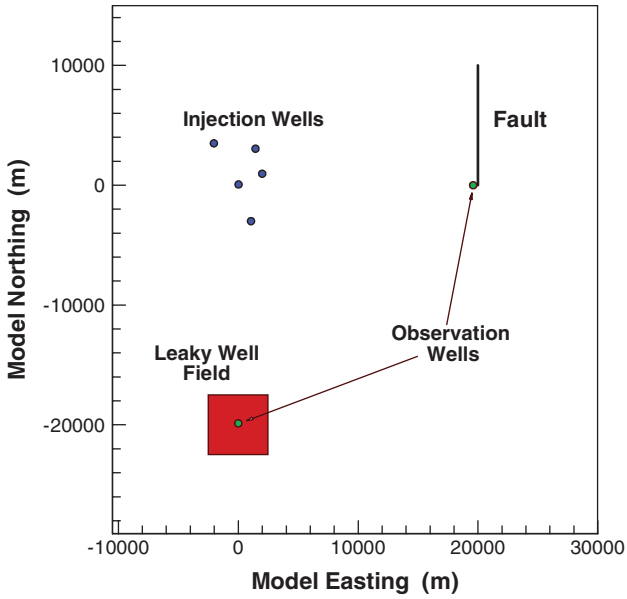

Figure 5. Schematic of the hypothetical case study for the application of Cihan et al. (2011) analytical solution.

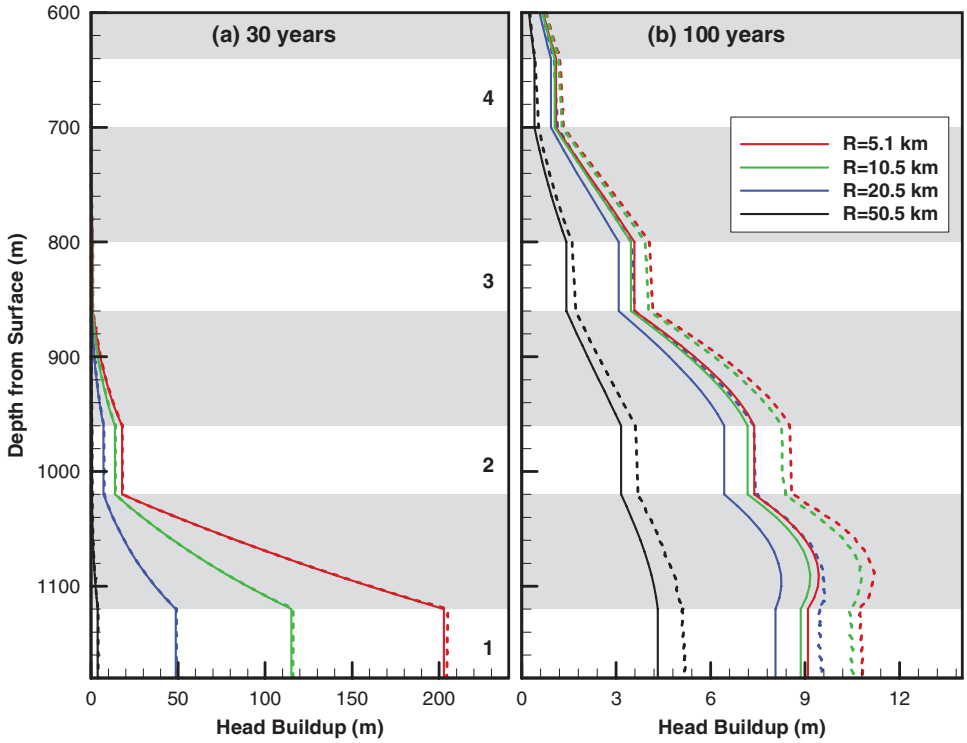

Figure 4. Vertical profiles of head buildup for different radial distances from the injection well at (a) 30 years and (b) 100 years. Dashed lines represent the numerical simulation results; solid lines represent the analytical solution results.

Application of the Analytical Solution to a Hypothetical Storage Case

This section presents application of our analytical solution for estimating far-field pressure buildup and fluid leakage in a hypothetical CO_2 sequestration scenario. We consider industrial-scale CO_2 storage in the bottom saline formation of a multilayered aquifer-aquitard system with multiple injection wells, multiple leaky wells, and a leaky fault, as shown in Figure 5. The vertical sequence of aquifers and aquitards, as well as the formation and fluid properties, are the same as in the comparison example in the previous section (Figure 1), except that the permeability of the aquifers is 3×10^{-13} m^2. Five million tons of CO_2 per year are injected for a time period of 50 years through five injection wells located in the vicinity of the domain origin. The single-phase equivalent-volume injection rate at each well is 3343 m^3/d (based on a CO_2 density of 820 kg/m^3). Three application scenarios are considered. The first scenario considers diffuse leakage through the aquitards, but does not involve any focused leakage pathways. The second scenario, in addition to diffuse leakage, investigates focused leakage occurring through a leaky well field that involves multiple wells in a rectangular zone with 5×5 km dimensions. The center of the well field is at a 20 km distance from the origin, south of the injection well area. The last scenario involves a leaky fault zone extending in a north-south direction, located 20 km east of the injection well area. The leaky fault zone is 10 km long and 200 m wide.

The Effects of Diffuse Leakage Through Aquitards on Pressure Buildup

In this scenario, we consider diffuse leakage through aquitards without any leaky wells or faults. We investigate injection-induced pressure perturbations and the corresponding brine migration in the aquifers (horizontally) and aquitards (vertically). Figure 6 demonstrates the strong sensitivity of total diffuse leakage rates to aquitard permeability. As mentioned above, the diffuse leakage rate is the rate of vertical flow between aquifers and aquitards within the multilayered system, integrated over the model domain. Compared to the base-case aquitard permeability of $k' = 10^{-18}$ m^2, a one-order-of-magnitude decrease in permeability reduces the maximum diffuse leakage rate from the storage formation into the overlying aquitard (Aquifer 1 to Aquitard 1) by about 43% for 50 years of injection. In contrast, increases in aquitard permeability from $k' = 10^{-18}$ m^2 to 10^{-17} m^2 result in a 22% increase in the maximum diffuse leakage rate from the storage formation. While brine leakage into Aquifers 5, 6, 7, and 8 is negligible for $k' = 10^{-18}$ or 10^{-19} m^2, deeper fluids are migrating into these freshwater aquifers at non-zero rates when aquitard permeabilities are equal to 10^{-17} m^2 or higher.

In Figure 7, vertical profiles of head buildup are given at an observation well (Easting = 0, Northing = −19,872 m, Figure 5) near the center of the leaky well field (to be considered later) for 50 years (end of injection period) and 100 years. The observation point also has the same distance from the origin to the observation well at the edge of the fault zone represented by the leaky wells in a following section. Results are presented using aquitard permeability values of $k' = 10^{-17}$, 10^{-18}, and 10^{-19} m^2. Also shown are results for $k' = 0$ (no vertical communication between layers), which is essentially the Theis solution applied to the storage formation (Theis 1935). Comparison of the different calculation cases demonstrates the important mitigating effect that low but non-zero aquitard permeabilities can have on the pressure buildup in the storage formation. The maximum head buildup observed in Figure 6 is about 210 m for the case without vertical communication, a value that reduces to about 125 m for the base case with $k' = 10^{-18}$ m^2, and to less than 60 m for the case with $k' = 10^{-17}$ m^2. This pressure relief by fluid leakage through aquitards has positive effects, such us reduced failure risk, increased storage capacity, and smaller area of review for site characterization.

At 100 years (right, Figure 7), head buildup in the storage formation has reduced significantly compared to the end-of-injection conditions, a result of continued lateral (within the aquifers as head changes propagate away from the injection location) and vertical (through diffuse leakage overlying aquifers and aquitards) equilibration. In two calculation cases (i.e., $k' = 10^{-19}$ m^2 and less

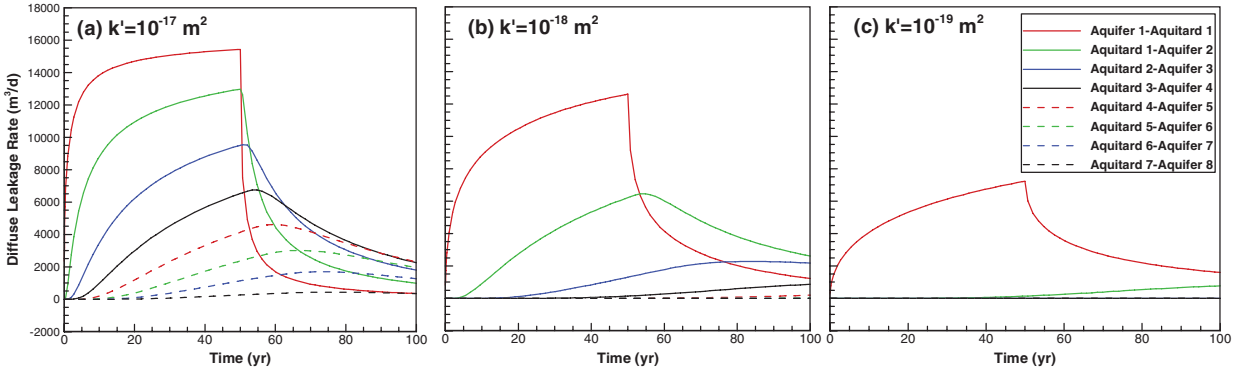

Figure 6. Sensitivity of diffuse leakage rates to changes in aquitard permeability for a scenario without any leaky well or fault.

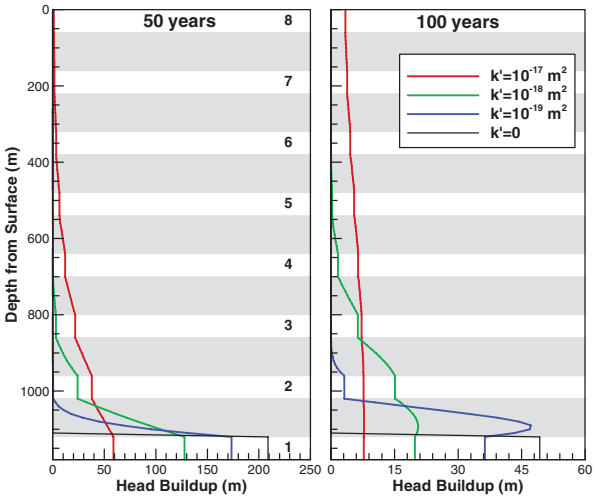

Figure 7. Vertical profiles of hydraulic head at an observation point close to the center of the well field (without any focused leakage), presenting sensitivity to aquitard permeability.

clearly $k' = 10^{-18}$ m^2), the primary caprock (Aquitard 1) recharges into the overlying and underlying aquifers, as indicated by the concave shape of the head buildup profiles. After injection ceases, the drop in hydraulic head is much faster in the aquifers compared to the aquitards, so that reverse gradients occur at certain locations and times.

Effect of Well Leakage on Pressure Buildup

We now look at the potential effects of a large number of abandoned wells situated about 20 km south from the five injection wells (Figure 5), a legacy of oil and gas exploration in the area. We assume that a subset of these wells is acting as pathways for focused leakage. As a base case, we use 36 leaky wells, arranged in a regular pattern in a well field of 5 × 5 km size. For simplicity, we distinguish between two general types of leaky wells, and we assume that all the leaky wells in the field have the same characteristics and properties.

The first leaky well type constitutes a very conservative case in terms of leakage potential and impact; here we assume that open wells connect the storage aquifer directly with the four freshwater aquifers (Aquifers 5, 6, 7, and 8), a scenario considered in the recent guidance document on regulation of CO_2 projects in the United States (USEPA 2011). The wells have very low resistance (well permeability is 10^{-5} m^2) and a radius of 0.076 m. Brine migrating from the storage formation up the wells has no hydraulic interaction with the overlying saline aquifers 2, 3, and 4, assuming that these well sections are cased.

The second well type considers an arguably more realistic and common scenario, with potential leakage pathways occurring in the annulus outside of the well casing. During the drilling process, the annular space between the casing and the borehole is generally filled with a cement material. A disturbed or damaged zone will typically form in the immediate vicinity of the well casing, from mechanical impacts during drilling, from imperfections within the cement and along the cement-formation interface, or from long-term degradation (Nelson 1990; Gasda et al. 2008). (Note that data on the geometry and properties of the disturbed zone outside of the well casing are hard to find in the literature.) We assume here that the radius of the disturbed zone surrounding the leaky well is 0.5 m, and we consider a range of effective permeabilities of the disturbed zone between 10^{-9} and 10^{-12} m^2. While these values are orders of magnitude lower than in the open wellbore case discussed above, they correspond to the upper range of well permeabilities discussed in previous studies (Watson and Bachu 2008, 2009; Nordbotten et al. 2009; Celia et al. 2011). In contrast to the first well type, brine migrating upward in the leaky pathway outside of the casing is interacting with all intervening aquifers.

Leakage Through Open Wells

We investigate here the extreme case of a well field with 36 high-permeability open wells. Figure 8a presents rates of focused leakage from the storage formation (Aquifer 1) into all 36 leaky wells (negative values) and from the 36 leaky wells into each of the freshwater aquifers—Aquifers 5, 6, 7, and 8 (positive values). (Note that since the analytical solution neglects storage in leaky wells, and since the wells have a no-flow boundary condition at the top and the bottom, the focused-leakage rate out of the storage formation is equal to the sum of the rates of leakage into Aquifers 5, 6, 7, and 8.) The focused leakage is significant in this scenario; at the end of injection, the total brine flow rate leaving the storage formation via focused leakage amounts to about 21% of the volumetric CO_2 injection rate. The brine volume leaving Aquifer 1 through well leakage is redistributed into Aquifers 5, 6, 7, and 8, with the highest flow rate into Aquifer 5 (the deepest freshwater aquifer) and the minimum flow rate into the uppermost Aquifer 8. This gradual decrease in the vertical direction, a result of the fluids lost into intervening aquifers, has been described earlier for focused leakage in aquifers with impermeable aquitards (Nordbotten et al. 2004; Cihan et al. 2011). Nordbotten et al. (2004) introduced the term "elevator effect" for this behavior, because the leakage rate through wells decreases monotonically with increasing vertical distance from the storage aquifer. We observe the same elevator effect here for multilayered systems with diffuse leakage through permeable aquitards.

The presence of the leaky well field generates considerable changes in the head distributions throughout the multilayered domain. Figure 9a shows the spatial distribution of head changes after 50 years of fluid injection. The focused leakage in the high-permeability wells causes a head drawdown in the storage formation centering on the well field, while large-scale head increases of up to 30 m are generated in Aquifer 5 (the deepest freshwater aquifer). Figures 10a and 11a present transient changes and vertical profiles, respectively, for head buildup at the observation point close to the

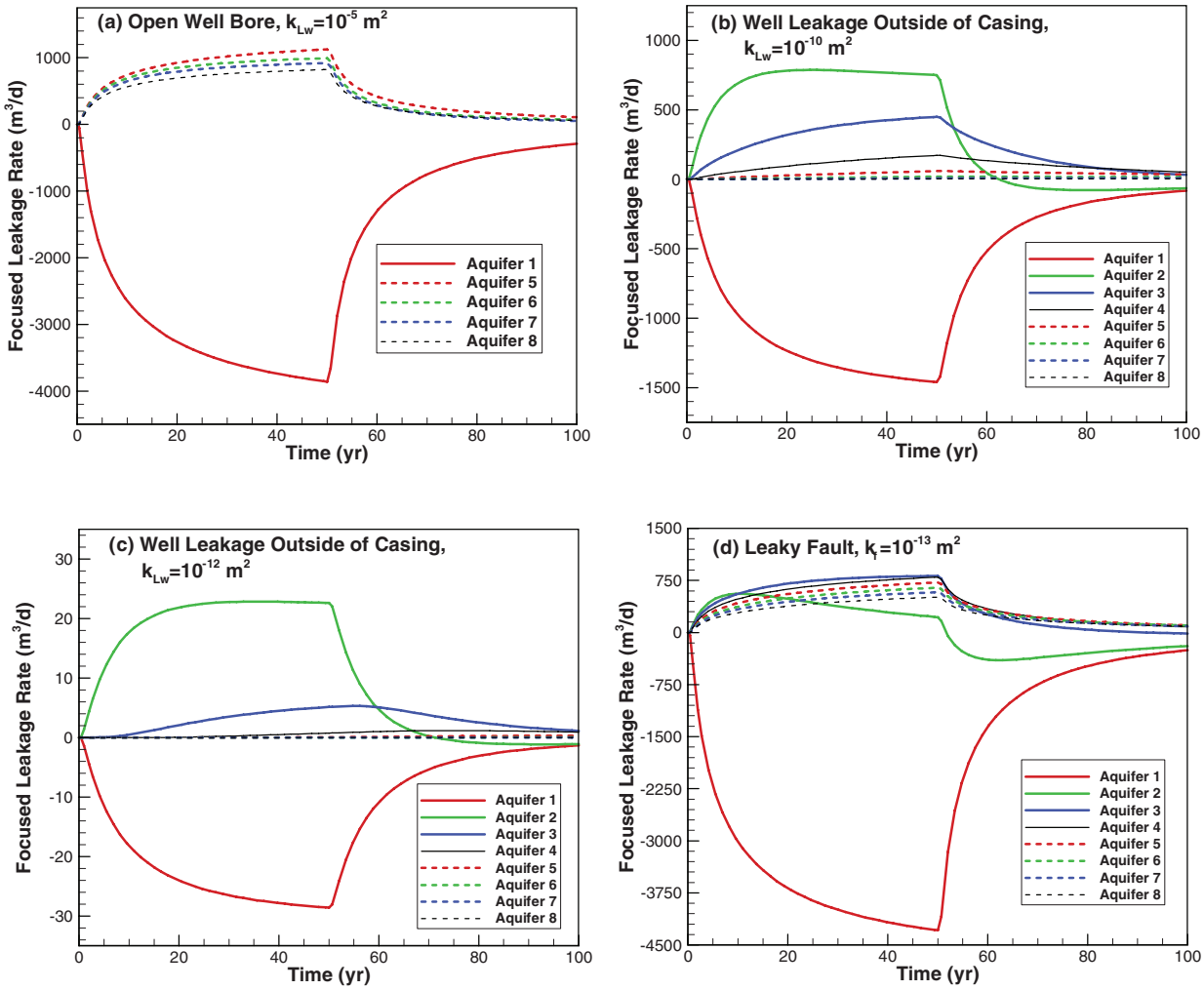

Figure 8. Rate of focused leakage into aquifers as a function of time for different leakage paths. (a) Cased open wellbores between the storage formation and the freshwater aquifers with very small flow resistance, (b and c) leakage through disturbed zones outside of well casings, and (d) leakage through a leaky fault represented by 39 leaky wells. The number of the wells in the well field for (a) through (c) is 36. Positive leakage rates are from wells (fault) into aquifers; negative leakage rates are from aquifers (fault) into wells.

center of the leaky well field. Again, we observe that focused leakage significantly decreases the head buildup in the storage reservoir compared to the scenario without the leaky well field ($k_{LW} = 0$), while strongly affecting the freshwater aquifers, both during the injection and post-injection periods. The overlapping dashed lines in Figure 10a suggest that the extremely permeable flow paths allow for vertically equilibrated head changes along all the freshwater aquifers at this location. This can also be seen in the vertical profiles of head buildup in Figure 11a, which show identical head changes in the top four aquifers. Notice the retardation in the response of the upper three aquitards in the vertical head profiles. At 50 years, the head buildup in these aquitards is slightly less than in the neighboring aquifers, indicating that local aquifers discharge into the aquitards. We see the opposite effect at 100 years during the post-injection period, since the aquitard head increases are higher, and the aquifers are locally recharged by flow from the aquitards.

Leakage Through Well Annulus

The second well-leakage scenario is identical to the previous case with regard to well location and number of wells, but assumes that flow occurs through microcracks or fractures in the disturbed zone around a cased wellbore. Effective well permeabilities expected for this scenario are much lower than in the open wellbore case (Watson and Bachu 2008; Celia et al. 2011). It is also assumed that the leaking brine may interact laterally with all intervening aquifers encountered along the flow path. Figure 8b and 8c presents the total flow rates between the 36 leaky wells and the 8 aquifers of the multilayered domain for effective well permeabilities of $k_{LW} = 10^{-10}$ m^2 and $k_{LW} = 10^{-12}$ m^2, respectively. Compared to the open wellbore case (Figure 8a), brine leaves the storage formation at a significantly reduced rate, with a maximum of about 550 m^3/d (3% of injection rate) for $k_{LW} = 10^{-10}$ m^2 and a maximum of about 28 m^3/d (0.2% of injection rate) for $k_{LW} = 10^{-12}$ m^2. Since the leaky flow paths communicate with *all* aquifers, the major fraction of the

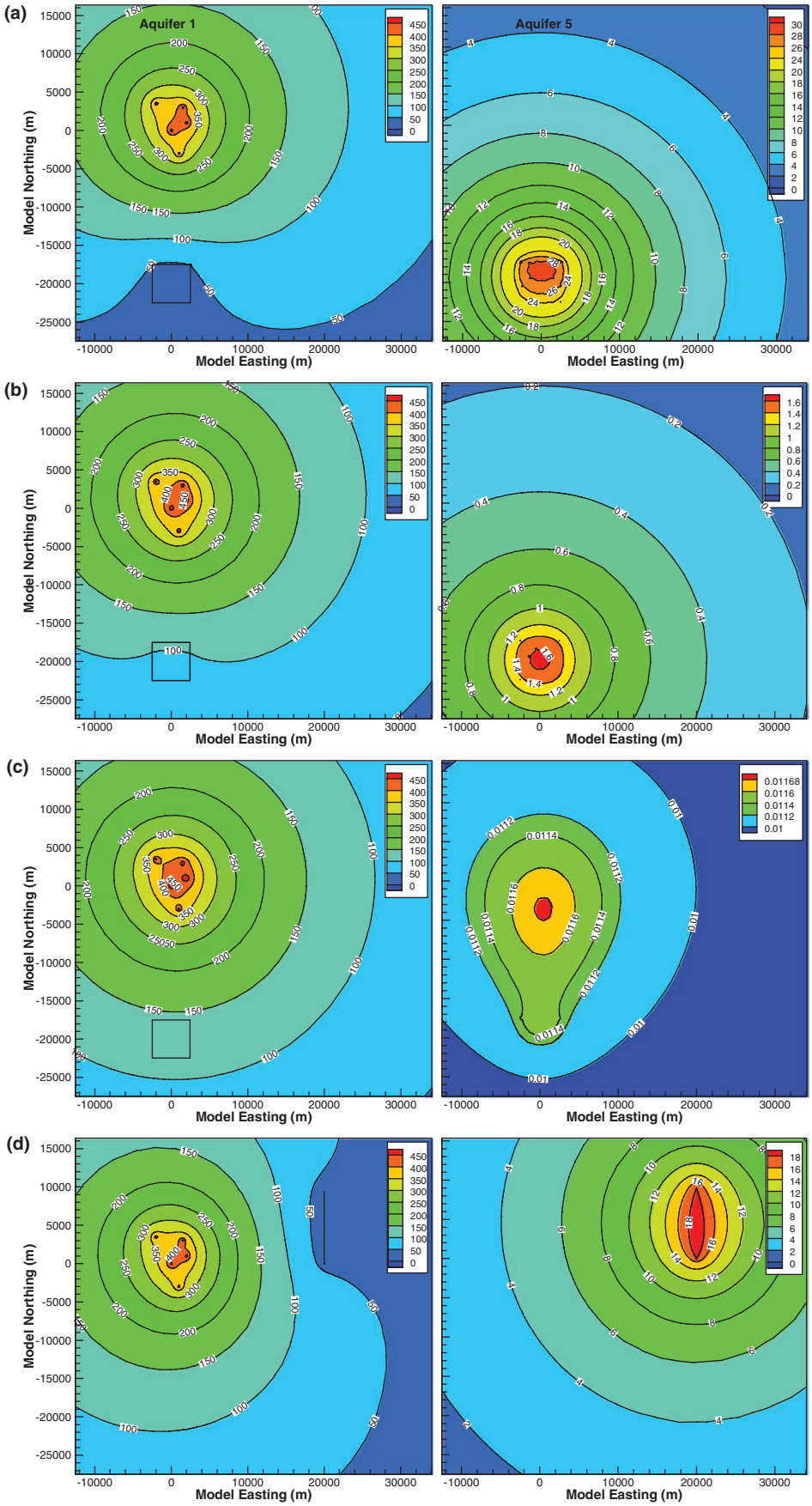

Figure 9. Contour plot of hydraulic head buildup (m) in Aquifer 1 (left) and Aquifer 5 (right) for (a) open wellbore case, (b through c) well leakage outside of casing with $k_{LW} = 10^{-10}$ to 10^{-12} m^2, respectively, and (d) leaky fault ($k_f = 10^{-13}$ m^2).

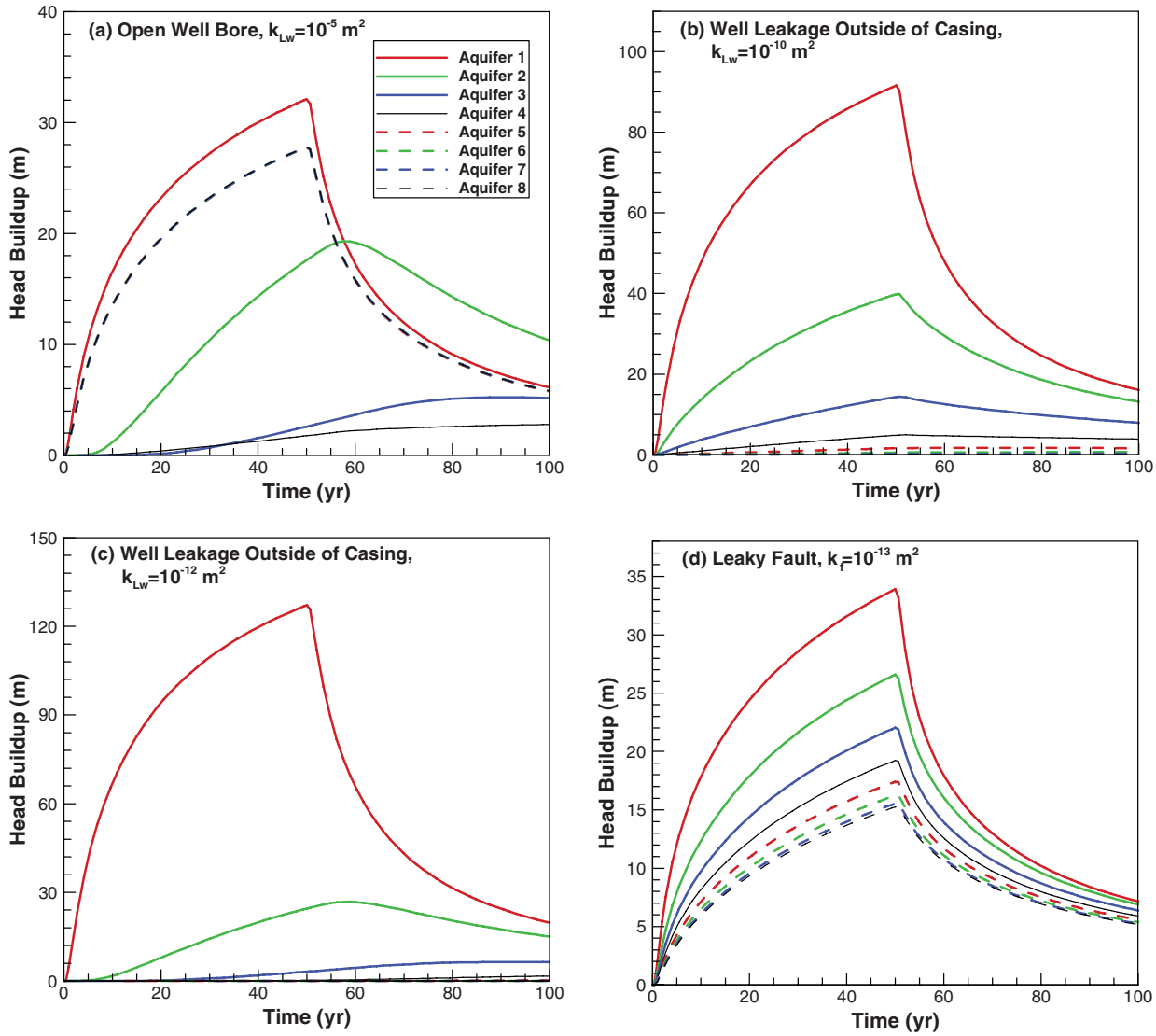

Figure 10. Head changes in aquifers as function of time for three different scenarios. In (a) and (b) head buildup shown near the center of the leaky well field (Easting = 0, Northing = −19,872 m, that is about 623 m from the nearest leaky well), and in (c) near the fault (19,872 m, 0), that is approximately at the edge of a representative leaky well with 127.32 m radius in the fault zone. All dashed lines in (a) overlap.

brine leaving the storage formation recharges into the nearest overlying layers, in this case the saline aquifers 2, 3, and 4. As a result of this elevator effect, leakage into the shallow aquifers (Aquifers 5, 6, 7, and 8) is very small. The maximum rate into Aquifer 5 during the 100 years of time is 60 m^3/d for $k_{LW} = 10^{-10}$ m^2 and only about 0.3 m^3/d for $k_{LW} = 10^{-12}$ m^2.

It is worth noting in Figure 8b and 8c that the flow rate between the leaky wells and Aquifer 2 becomes negative during the post-injection period, indicating that flow actually occurs from this aquifer into the wells. Because of ongoing diffuse leakage from the storage formation through Aquitard 1, the head buildup in Aquifer 2 is large enough to create a gradient toward the leaky wells, such that the flow direction reverses during the post-injection period. Both Aquifers 1 and 2 then feed into the leaky wells, while Aquifers 3, 4, 5, 6, 7, and 8 are receiving fluids. Such effects can only be represented in a calculation/simulation that accounts for both the diffuse brine migration through aquitards and the focused brine leakage through wells.

Figure 9b and 9c shows head change contours for the two leaky well cases; Figure 10b and 10c gives the corresponding transient changes in head buildup at the observation point near the center of the well field. In both well permeability cases, the spatial patterns of head increase in the storage formation are not significantly affected by well leakage (Figure 9b and 9c). Because of the relatively small leakage rates and the brine losses into intervening layers, the head changes in Aquifer 5 are also quite modest; the higher effective permeability of 10^{-10} m^2 results in a maximum head increase of less than 2 m in the center of the leaky well field, whereas the lower effective permeability of 10^{-12} m^2 shows less than 0.01 m head response. In the latter case,

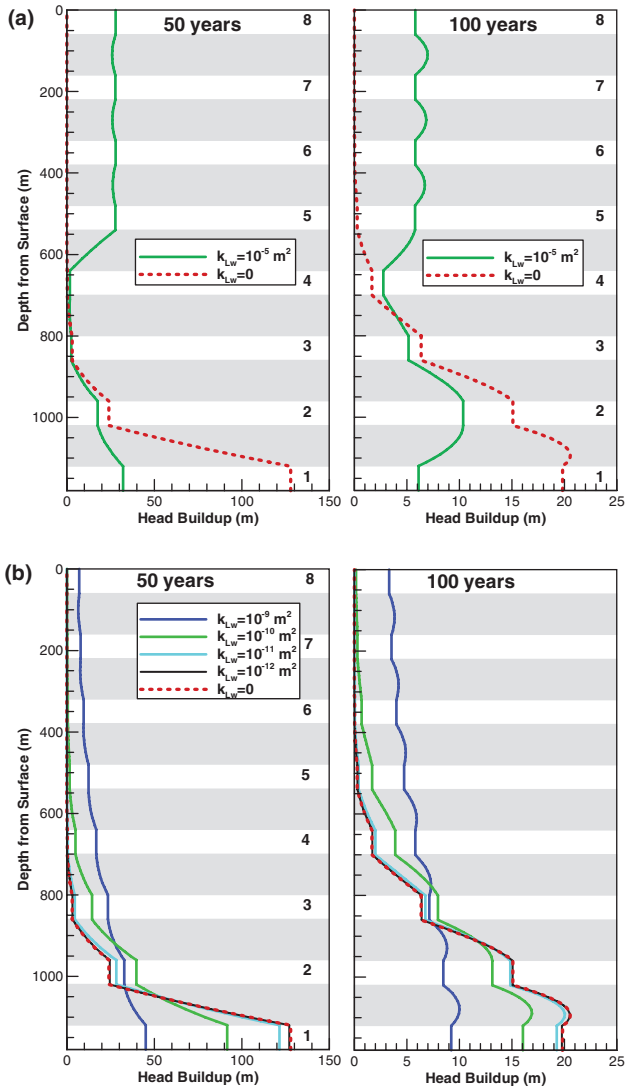

Figure 11. Vertical profiles of head buildup (Easting = 0, Northing = −19,872 m) comparing the results of several well permeability cases for (a) open wellbore scenario and (b) scenario for leakage through a disturbed zone outside of well casing.

the head change near the leaky well field, caused by well leakage, is similar in magnitude to the head change above the injection well field, caused by diffuse leakage only.

Vertical profiles of head change near the center of the leaky well field are compared in Figure 11b for a range of effective well permeabilities from 10^{-9} m^2 to 10^{-12} m^2, as well as for a case without any well leakage. The profiles confirm that the shallow freshwater aquifers are affected by well leakage only when the well permeability is extremely high for the type of well leakage considered in this section. The profile curves for $k_{LW} = 10^{-11}$ m^2 and $k_{LW} = 10^{-12}$ m^2 almost overlap with the profile curve for the scenario without leaky wells, suggesting that no significant head changes should be expected in shallow formations when realistic permeability cases are evaluated.

Effect of Well Density on Focused Leakage

The analyses of leakage processes in previous two sections are based on a well density of 36 leaky wells per 25 km^2. In this section, we change the number of leaky wells in the 5 × 5 km zone to investigate well density effects, in each case maintaining a regular well pattern. Figure 12a shows the focused leakage rate for the open wellbore case as a function of well density. While there is a strong increase in total leakage rate for small well numbers (i.e., less than 10 wells over the entire 25 km^2 well field), the leakage-vs.-well-density curve at higher well number shows asymptotic behavior. In other words, further increases in well density do not result in corresponding leakage-rate increases, as the lateral conductivity of the storage formation becomes the limiting factor in bringing fluids to the leaky well domain. Asymptotic behavior is seen when well density is higher than about three to four wells/km^2 at 50 years and about one well/km^2 at 100 years. The maximum total leakage rate (∼4100 m^3/d at 50 years) from the storage reservoir amounts to ∼25% of the total injection rate.

Stronger sensitivity to well density is observed for the well type with leakage occurring through fractures in the annulus outside of the well casing (Figure 12b), resulting from the much lower permeabilities associated with this type of well. The total leakage rate from the storage formation is nowhere near asymptotic behavior, even for well densities above 5 wells/km^2. Notice that at the end of injection, the focused leakage rate into Aquifer 2 has a local maximum at about 2.5 wells/km^2. In other words, the total leakage rate into this first aquifer overlying the storage formation initially increases with well density, but then starts decreasing (above 2.5 wells/km^2),although more leaky wells are added. Addition of leaky wells beyond 2.5 wells/km^2 and diffuse leakage through Aquitard 1 further increase head buildup locally around the leaky wells, and this in turn decreases head gradient between well-aquifer segments 1 and 2, resulting in less focused leakage into Aquifer 2. Although not shown here, a similar effect occurs at 100 years where the focused leakage rate into Aquifer 3 exhibits a local maximum at about 1.5 wells/km^2. Besides, both Aquifers 1 and 2 exhibit negative leakage rates during the post-injection period, indicating that flow actually occurs from these aquifers into the wells.

Effect of Fault Leakage on Pressure Buildup

This section demonstrates that our analytical solution may also be used to approximate vertical leakage in a conductive fault zone. On the basis of the assumptions detailed previously, the fault zone of 10 km length (L) and 200 m width (W) is represented by 39 leaky wells [$\cong L\pi/(4\ W)$], each having a radius of 127.32 m ($= 2W/\pi$). The vertical permeability along the fault is assumed to be uniform, and thus all the leaky wells representing the fault zone have identical permeability values. The fault zone is in hydraulic communication with all aquifers of the multilayered system.

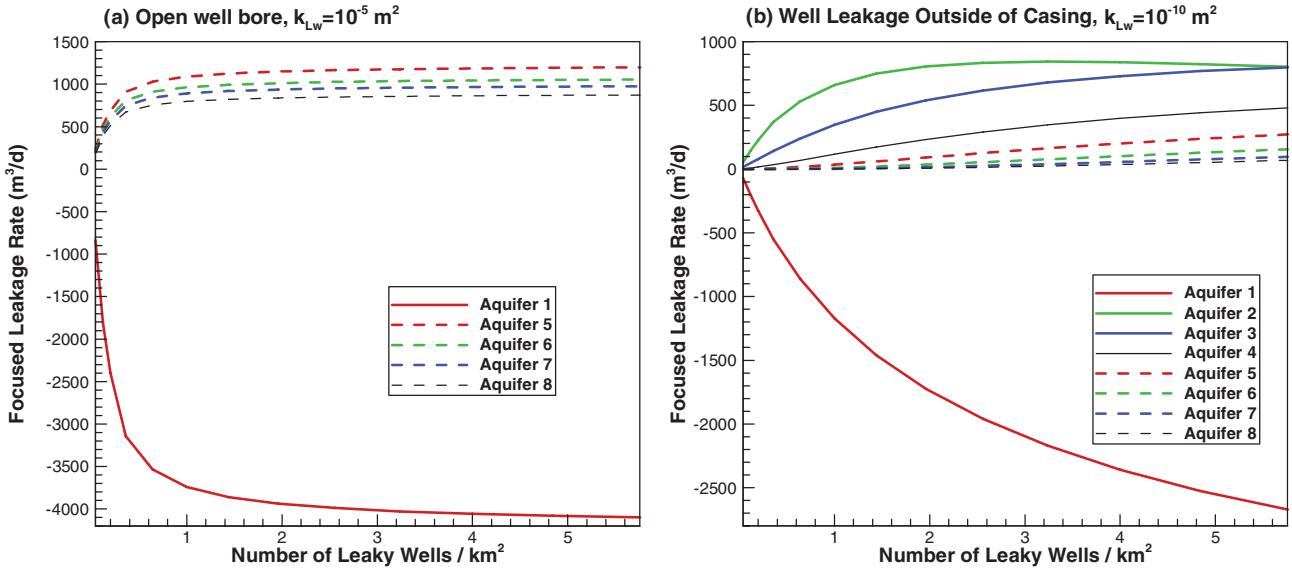

Figure 12. The effect of leaky well density on the total focused leakage rate in aquifers at 50 years. (a) Open wellbore scenario, and (b) Scenario of leakage through disturbed zone outside of well casing. The permeability of each leaky well is 10^{-10} m^2.

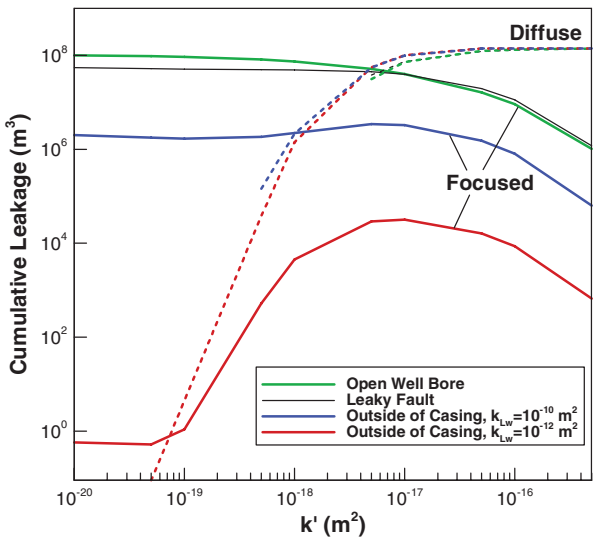

Figure 13. Cumulative leakage into the freshwater aquifers (Aquifers 5, 6, 7, and 8) over 100 years for four different scenarios. Solid lines indicate the cumulative focused leakage through leaky wells or leaky fault, and the dashed lines indicate the cumulative vertical diffuse leakage beneath the deepest freshwater aquifer (at Aquitard 4-Aquifer 5 interface).

Figure 8d shows flow rates between the fault zone and the aquifers for a fault-zone permeability of $k_f = 10^{-13}$ m^2; negative values indicate flow from the aquifer into the fault, whereas positive values indicate flow from the fault into the aquifers. The total leakage rate from the storage formation into the fault is significant in this case, constituting more than 24% of the total injection rate. Considerable brine leakage occurs into Aquifers 5 through 8, demonstrating that the presence of a major conductive fault zone can impact freshwater aquifers. Interestingly, the leakage rate into Aquifer 2 (the next aquifer above the storage formation) increases during the first 10 years of injection, but then gradually decreases for the remainder of the injection period, and finally becomes negative after injection stops. Aquifer 2 is subject to head increases from both local leakage within the fault (with immediate effects) and diffuse leakage through the aquitard (retarded response caused by low aquitard permeability), which with time reduces the driving force for flow from the fault into Aquifer 2. The driving force for flow in overlying aquifers is less affected because the impact of diffuse leakage is most prominent in Aquifer 2. As injection ceases, the continued diffuse leakage from the storage formation maintains the head increases in Aquifer 2 at a high enough level to revert the gradient toward the fault zone, so that Aquifer 2 starts discharging into the fault. A similar interplay between focused and diffuse leakage was seen earlier in leakage through wells.

The contours of head buildup in Figure 9d exhibit strong areal drawdown in the storage formation as a result of fault leakage, compared to a scenario without a fault. Similarly, we see spatially extensive head buildup in Aquifer 5 originating from the fault zone. The leaky fault creates an elliptical head buildup contour that is quite different from the other cases. Comparison of the transient head buildup in Figure 10d (at an observation point close to the fault) with the well leakage scenarios in Figure 10a through 10c shows that the local hydraulic response is more equilibrated between all aquifers, as a result of significant leakage through the fault and full hydraulic communication with the aquifers.

Discussion

Analyses of diffuse leakage only in response to CO_2 injection into the bottom aquifer of the eight-aquifer-seven-aquitard system show that the shallow freshwater

aquifers start exhibiting moderate head buildup only when aquitard permeability is 10^{-17} m^2 or higher, suggesting that the effect of diffuse leakage could extend into shallower formations when aquitard permeability is relatively high. The head buildup for $k' \geq 10^{-17}$ m^2 could have an impact on the shallow groundwater regime and affect groundwater interaction with surface water sources. However, Birkholzer et al. (2009), simulating salinity changes, showed that such vertical migration of brine through the sequence of low-permeability aquitards is not a concern to water quality, because even if the total vertical flow rates were large (because of integration over large domains), the associated vertical transport velocities ($\leq$0.006 m/year for $k' \leq 10^{-16}$ m^2) were almost negligible. As a result of these low advective velocities, their simulated vertical profile of salinity remained almost unchanged over a 100-year time period. With respect to possible groundwater quality issues, the flow of brine (plus other contaminants) through focused leakage paths is of concern (Birkholzer et al. 2009).

Figure 13 shows the cumulative leakage into the freshwater aquifers (Aquifers 5, 6, 7, and 8) over 100 years through different leakage paths as a function of aquitard permeability, for the scenarios discussed in the previous sections. Solid lines indicate the cumulative focused leakage through leaky wells or a leaky fault, and the dashed lines indicate the cumulative vertical diffuse leakage beneath the deepest aquifer (at the Aquitard 4-Aquifer 5 interface) corresponding to the four different scenarios plotted. Note that the cumulative leakage is plotted in the log-scale, and that some dashed lines are not continuous because the diffuse leakage rate becomes negative for certain scenarios and aquitard permeability values (i.e., flow occurs from Aquifer 5 to the underlying Aquitard 4).

The presence of 36 leaky open wellbores nearby a CO_2 injection site constitutes an extreme scenario for evaluating the effect of leakage on groundwater quality because they provide direct vertical paths with negligibly small resistance ($k_{LW} = 10^{-5}$ m^2) for transfer of poor quality water from the storage aquifer into the freshwater aquifers. The driving force for the vertical transport of salt water along the open wellbore is the head gradient. The cumulative leakage over 100 years into the freshwater aquifers takes its maximum value when the head buildup is the greatest in the storage aquifer, which corresponds to the case with the lowest caprock (aquitard 1) permeability, that is, $k' \rightarrow 0$ (Figure 13). The leakage decreases when the aquitard permeabilities are $\geq 10^{-17}$ m^2, where the diffuse leakage becomes dominant over the focused leakage. The presence of a major conductive fault zone with a vertical permeability of $k_f = 10^{-13}$ m^2 results in similarly high focused cumulative leakage into the freshwater aquifers over 100 years (in the order of 10^8 m^3).

The leakage behavior for flow through microcracks or fractures in the disturbed zone around cased wellbores is quite different. Effective well permeabilities are much lower than in the open wellbore case, and the leaking brine interacts laterally with all intervening aquifers encountered along the flow path. In contrast to the open wellbore case, the maximum cumulative leakage into the freshwater aquifers from 36 leaky wells over 100 years ($\sim$32,000 m^3 for $k_{LW} = 10^{-12}$ m^2, and 3.5 million m^3 for $k_{LW} = 10^{-10}$ m^2) occurs when the aquitard permeability is between 10^{-17} and 10^{-18} m^2. The leakage from the leaky wells into the freshwater aquifers is controlled by the head difference at the leaky well-aquifer segments between Aquifer 4 and Aquifer 5. Small head differences and the leaky wells with high resistances result in low cumulative focused leakage for $k_{LW} = 10^{-12}$ m^2. The diffuse leakage through the deep aquifers increasing with aquitard permeability causes the head gradient between Aquifers 4 and 5 to change. The cumulative focused leakage increases with increasing head gradient and takes its maximum value when the head difference between the leaky well-aquifer 4 and the leaky well-aquifer 5 (the deepest aquifer) segments becomes maximum for an aquitard permeability between 10^{-17} and 10^{-18}m^2. When the aquitard permeability is $\geq 10^{-17}$ m^2, significantly high diffuse leakage rates cause head more or less equilibrate between the aquifers (Figure 7), and thus the cumulative focused leakage decreases in Figure 13. If one assumes that the leaked brine will mix with freshwater over the 60 m thickness of the aquifers with 0.2 porosity, in response to the 32,000 m^3 brine leakage into the four freshwater aquifers for $k_{LW} = 10^{-12}$ m^2, the radius of the affected area at each aquifer around each leaky well is less than 4 m. It is valuable to compare these leakage scenarios with effective permeability values for abandoned wells reported in the literature. Watson and Bachu (2008, 2009) presented an attempt to classify abandoned wells with respect to leakage potential. Their qualitative approach classified wells into four categories with, respectively, extreme, high, medium, and low leakage potential, using soft data such as well type, depth, year, completion report, and type of abandonment. Celia et al. (2011) mapped their well score classification (Watson and Bachu 2008) to effective well-permeability ranges for leakage occurring in the disturbed zone around a wellbore. According to their mapping, wells with very high leakage potential would correspond to an effective permeability range from 10^{-11} m^2 to 8×10^{-15} m^2, wells with high leakage potential would correspond to a range from 8×10^{-15} m^2 to 5×10^{-16} m^2, and wells with medium leakage potential would correspond to a range from to 5×10^{-16} m^2 to 2×10^{-17} m^2. Thus, the 10^{-12} m^2 effective permeability case studied here represents very high leakage potential according to Celia et al. (2011); yet the rate of brine leakage into the freshwater aquifers appears to be rather marginal in terms of potential water quality impacts.

Summary and Conclusions

To study large-scale head changes and brine flow rates in a leaky aquifer-aquitard system, we applied a recently developed single-phase analytical solution to a hypothetical CO_2 sequestration scenario involving multiple injection wells, multiple leaky wells, and a leaky fault. The

basic assumption is that brine migration processes at distances beyond the CO_2 plume region can be reasonably well described by single-phase flow models without accounting for local two-phase and variable density effects that occur within the plume region. In our example scenario, we consider injection of 5 million tons of CO_2 via five injection wells, represented by a single-phase equivalent-volume injection rate of 3343 m^3/d at each well. Pathways for focused leakage are at a distance of about 20 km from the injection well field, which is much farther than the maximum CO_2 plume extent to be expected for this scenario. We used the demonstration application to (1) elucidate the pressure response in the layers of the aquifer-aquitard stratigraphic sequence, including the storage formation, the three overlying saline aquifers, and the top four freshwater aquifers, (2) to illustrate the complex interplay between diffuse and focused leakage, and (3) to evaluate the sensitivity of head changes and leakage rates to aquitard and well permeabilities. It should be pointed out that the selected leakage scenarios do not necessarily reflect realistic conditions expected in CO_2 sequestration projects; they have in part been chosen to demonstrate the usefulness of our solution even for extreme cases. A leaky well field with a large number of open wellbores, for example, is surely a scenario that should not be expected in the vicinity of a real CO_2 storage site. Similarly, it may be very unlikely to encounter leaky faults that traverse hundreds of meters of alternating shale and reservoir rock.

To verify our assumption that the detailed multiphase flow processes within the two-phase zone have negligible impact on the far-field conditions, we compared the analytical solution results against a CO_2 sequestration simulation study from the literature (Birkholzer et al. 2009). The results confirmed that both the head changes and brine flow rates outside of the CO_2 plume were approximated with reasonable accuracy by a single-phase flow model. We may conclude that the analytical solution applied in this study is an efficient quick-assessment tool for analyzing far-field pressure buildup in response to CO_2 storage, in complex multilayered systems with leakage potentially occurring through multiple aquitards, multiple leaky wells, and/or a leaky fault. Because of its high efficiency in obtaining results, the analytical solution could be particularly useful for uncertainty quantification, parameter estimation, or for the optimization of pressure-management schemes (Birkholzer et al. 2012), as long as the assumptions behind it are in accord with those of reasonably simplified actual problems.

Acknowledgments

The authors wish to thank four anonymous reviewers, as well as Curtis M. Oldenburg of Lawrence Berkeley National Laboratory (LBNL), for their careful review of the manuscript and the suggestion of improvements. This work was funded in part by the USEPA, Office of Water and Office of Air and Radiation, under an Interagency Agreement with the U. S. Department of Energy (USDOE) at LBNL. Supplementary funding was provided by the Assistant Secretary for Fossil Energy, Office of Sequestration, Hydrogen, and Clean Coal Fuels, through the National Energy Technology Laboratory, under the USDOE contract DE-AC02-05CH11231. The FORTRAN code developed for computing the analytical solutions can be obtained from the authors upon request.

References

Bergmo, P.E., A. Grimstad, and E. Lindeberg. 2011. Simultaneous CO_2 injection and water production to optimize aquifer storage capacity. *International Journal of Greenhouse Gas Control* 5, 555–564.

Birkholzer, J.T., and Q. Zhou. 2009. Basin-scale hydrogeologic impacts of CO_2 storage: capacity and regulatory implications. *International Journal of Greenhouse Gas Control* 3, no. 6: 745–756.

Birkholzer, J.T., Q. Zhou, and C.-F. Tsang. 2009. Large-scale impact of CO_2 storage in deep saline aquifers: a sensitivity study on the pressure response in stratified systems. *International Journal of Greenhouse Gas Control* 3, no. 2: 181–194.

Birkholzer, J., A. Cihan, and Q. Zhou. 2012. Impact-driven pressure management via targeted brine extraction—concept studies of CO_2 storage in saline formations with leakage pathways, *International Journal of Greenhouse Gas Control* 7, 168–180.

Buscheck, T.A., Y. Sun, T.J. Wolery, W. Bourcier, A.F.B. Tompson, E.D. Jones, S.J. Friedmann, and R.D. Aines. 2011. Combining brine extraction, desalination, and residual-brine reinjection with CO_2 storage in saline formations: implications for pressure management, capacity, and risk mitigation. 10th International Conference on Greenhouse Gas Control Technologies, GHGT-10. *Energy Procedia* 4, 4283–4290.

Celia, M.A., and J.M. Nordbotten. 2009. Practical modeling approaches for geological storage of carbon dioxide. *Ground Water* 47, no. 5: 627–638.

Celia, M.A., J.M. Nordbotten, B. Court, M. Dobossy, and S. Bachu. 2011. Field-scale application of a semi-analytical model for estimation of CO_2 and brine leakage along old wells. *International Journal of Greenhouse Gas Control* 5, 257–269.

Cihan, A., Q. Zhou, and J. Birkholzer. 2011. Analytical solutions for pressure perturbation and fluid leakage through aquitards and wells in multilayered aquifer systems. *Water Resources Research* 47: W10504. DOI: 10.1029/2011WR010721.

Court, B., M.A. Celia, J.N. Nordbotten, and T.R. Elliot. 2011. Active and integrated management of water resources throughout CO_2 capture and sequestration operations. 10th international conference on greenhouse gas control technologies, GHGT-10. *Energy Procedia* 4, 4221–4229.

Freeze, R.A., and J.A. Cherry. 1979. *Groundwater.* Upper Saddle River, New Jersey: Prentice Hall, Inc.

Gasda, S.E., S. Bachu, and M.A. Celia. 2004. Spatial characterization of the location of potentially leaky wells penetrating a geological formation in a mature sedimentary basin. *Environmental Geology* 46, no. 6–7: 707–720. DOI: 10.1007/s00254-004-1073-5.

Gasda, S., J.M. Nordbotten, and M. Celia. 2008. Determining effective wellbore permeability from a field pressure test: a numerical analysis of detection limits. *Environmental Geology* 54, 1207–1215. DOI: 10.1007/s00254-007-0903-7.

Intergovernmental Panel on Climate Change (IPCC). 2005. Intergovernmental Panel on Climate Change (IPCC). In

Special Report on Carbon Dioxide Capture and Storage, ed. B. Metz, O. Davidson, H. de Coninck, M. Loos, and L. Mayer. Cambridge, UK/New York: Cambridge University Press.

Nelson, E.B. 1990. *Well Cementing (Developments in Petroleum Science).* Amsterdam, the Netherlands: Elsevier.

Neuman, S.P., and P.A. Witherspoon. 1969. Theory of flow in a two-aquifer system. *Water Resources Research* 5, no. 4: 803–816.

Nicot, J.P. 2008. Evaluation of large-scale CO_2 storage on freshwater sections of aquifers: an example from the Texas Gulf Coast Basin. *International Journal of Greenhouse Gas Control* 2, no. 4: 582–593.

Nordbotten, J.M., and M.A. Celia. 2006. Similarity solutions for fluid injection into confined aquifers. *Journal of Fluid Mechanics* 561: 307–327.

Nordbotten, J.M., M.A. Celia, and S. Bachu. 2004. Analytical solutions for leakage rates through abandoned wells. *Water Resources Research* 40. DOI: 10.1029/2003WR002997.

Nordbotten, J.M., D. Kavetski, M. Celia, and S. Bachu. 2009. Model for CO_2 leakage including multiple geological layers and multiple leaky wells. *Environmental Science And Technology* 43: 743–749.

Oldenburg, C.M., S.L. Bryant, and J.-P. Nicot. 2004. Certification framework based on effective trapping for geologic carbon sequestration. *International Journal of Greenhouse Gas Control* 3: 444–457.

Pacala, S., and R.H. Socolow. 2004. Stabilization wedges: solving the climate problem for the next 50 years with current technologies. *Science* 305, no. 5686: 968–972.

Person, M., A. Banerjee, J. Rupp, C. Medina, P. Lichtner, C. Gable, R. Pawar, M. Celia, J. McIntosh, and V. Bense. 2010. Assessment of basin-scale hydrologic impacts of CO_2 sequestration, Illinois Basin. *International Journal Of Greenhouse Gas Control* 4, no. 5: 840–854.

Pruess, K. 2005. ECO2N: A TOUGH2 fluid property module for mixtures of water, NaCl, and CO_2. Lawrence Berkeley Laboratory Report LBNL-57952, Berkeley, California.

Rutqvist, J., J.T. Birkholzer, F. Cappa, and C.-F. Tsang. 2007. Estimating maximum sustainable injection pressure during geological sequestration of CO_2 using coupled fluid flow and geomechanical fault-slip analysis. *Energy Conversion and Management Journal* 48, no 6: 1798–1807.

Rutqvist, J., J.T. Birkholzer, and C.-F. Tsang. 2008. Coupled reservoir–geomechanical analysis of the potential for tensile and shear failure associated with CO_2 injection in multilayered reservoir–caprock systems. *International Journal of Rock Mechanics and Mining Sciences* 45, no. 2: 132–143.

Shan, C., I. Javandel, and P. Witherspoon. 1995: Characterization of leaky faults: study of water flow in aquifer-fault-aquifer systems. *Water Resources Research* 31, no. 12: 2897–2904.

Stehfest, H. 1970a. Numerical inversion of Laplace transforms. *Communications of the ACM* 13, no. 1: 47–49.

Stehfest, H. 1970b. Remark on algorithm. Numerical inversion of Laplace transforms. *Communications of the ACM* 13, no. 10: 624.

Theis, C.V. 1935. The relation between the lowering of the piezometric surface head and the rate and duration of discharge of a well using ground-water storage. *Eos Transactions, American Geophysical Union* 16: 519–524.

United States Environmental Protection Agency (USEPA). 2011. Draft Underground Injection Control (UIC) Program Class VI Well Area of Review Evaluation and Corrective Action Guidance for Owners and Operators, EPA-816-D-10-007, March 2011, available online at http://water.epa.gov/type/groundwater/uic/class6/gsguidedoc.cfm

Van der Meer, L.G.H. 1992. Investigations regarding the storage of carbon dioxide in aquifers in the Netherlands. *Energy Conversion and Management* 33, no. 5–8: 611–618.

Watson, T.L., and S. Bachu. 2008. Identification of wells with high CO_2-leakage potential in mature oil fields developed for CO_2-enhanced oil recovery. In *Paper SPE 11294, SPE Improved Oil Recovery Symposium*, April 19–23. Tulsa, Oklahoma.

Watson, T.L., and S. Bachu. 2009. Evaluation of the potential for gas and CO_2 leakage along wellbores. *SPE Drilling & Completion* 24, 115–126.

Yamamoto, H., K. Zhang, K. Karasaki, A. Marui, H. Uehara, and N. Nishikawa. 2009. Numerical investigation concerning the impact of CO_2 geologic storage on regional groundwater flow. *International Journal Of Greenhouse Gas Control* 3, no. 5: 586–599.

Zhou, Q., and J.T. Birkholzer. 2011. On scale and magnitude of pressure build-up induced by large-scale geologic storage of CO2. *Greenhouse Gases: Science and Technology* 1, 11–20. DOI:10.1002/ghg3.001.

Zhou, Q., J.T. Birkholzer, E. Mehnert, Y.-F. Lin, and K. Zhang. 2010. Modeling basin- and plume-scale processes of CO_2 storage for full-scale deployment. *Ground Water* 48, no. 4: 494–514.